Ionized physical vapor deposition of integrated circuit interconnects*

J. Hopwood[†,a)]
Northeastern University, Boston, Massachusetts 02115

(Received 19 November 1997; accepted 25 November 1997)

Interconnects, once the technological backwater of integrated circuit technology, now dominate integrated circuit cost and performance. As much as 90 percent of the signal delay time in future integrated circuit designs will be due to the interconnection of semiconductor devices while the remaining 10 percent is due to transistor-related delay. This shifts the thrust of critical research toward an improved understanding of interconnect science and technology. Shrinking circuit geometries will require high aspect ratio (AR) vias to interconnect adjacent metal layers. By the year 2007 it is predicted that logic circuits will use 6 to 7 interconnected metal layers with via ARs of 5.2:1. Memory will need fewer layers, but ARs as high as 9:1. In this paper, the demands of interconnect technology will be reviewed and the opportunities for plasma-based deposition of vias will be discussed. One promising new method of fabricating high-aspect ratio vias is ionized physical vapor deposition (I-PVD). The technique economically creates a unidirectional flux of metal which is uniform over 200–300 mm diameter wafers. Since metal ejected by conventional sputtering is primarily neutral and exhibits a cosine angular velocity distribution, sputtered metal atoms do not reach the bottom of high AR vias. By sputtering these atoms into a moderate pressure (4 Pa), high-density Ar plasma, however, the metal atoms are first thermalized and then ionized. The ions are then readily collimated by the plasma sheath and directionally deposited into narrow, deep via structures. Experiments have consistently shown that over 80% of the metal species are ionized using I-PVD. The physical mechanisms responsible for ionization will be discussed from both an experimental and modeling perspective and the spatial variation of metal ionization is experimentally determined. © *1998 American Institute of Physics.* [S1070-664X(98)90405-0]

I. BACKGROUND: INTEGRATED CIRCUIT INTERCONNECT TECHNOLOGY

In the microelectronics revolution much attention has been focused on the rapidly increasing number of devices per chip and the shrinking critical dimensions of these electronic components. The explosion in the number of transistors fabricated on a single integrated circuit (IC), however, has placed extreme demands on electrically interconnecting these devices in the manner necessary to perform the logical operations of a modern microprocessor. Figure 1 shows a simplified, partial cross section of a typical IC. A single metal-oxide-semiconductor field effect transistor (MOSFET) is shown in the figure with gate (G), source (S), and drain (D) connections labeled. Interconnection of this MOSFET with other devices on the chip (not shown) is accomplished through the polysilicon/metal alloy (silicide) gate level and several metal-SiO_2 interlayer dielectric (ILD) levels joined together by vertical vias. Past generations of microprocessors used three metal levels as shown in Fig. 1, but designs using more transistors demand additional levels of metal. The National Technology Roadmap for Semiconductors[1] forecasts that 7 to 8 levels of interconnect will be required by 2010. With such a large number of layers it is clear that the fabrication of interconnects will dominate the process of manufacturing future ICs.

The electrical performance of an IC is most easily gauged by the maximum clock speed at which the chip operates reliably. The clock speed is determined by how quickly the transistors can be switched on and off as well as how quickly the signal propagates from one device to the next. As the interconnect scheme becomes more complex, the signal delay due to longer, thinner interconnect lines dominates the total switching time and, therefore, the maximum clock rate. In the most simple sense, the interconnect delay is determined by the product of the interconnect resistance (R) and the parasitic capacitance (C) of the interconnect metal to the adjacent layers.[2] The thickness of the ILD must remain constant in future ICs such that the interconnect capacitance does not become any larger. At the same time, however, the widths of the metal lines and vias will shrink to accommodate the greater density of transistors. The result is that the aspect ratio (AR) of interconnect vias may increase to approximately 9:1 as the lateral critical dimensions decrease to 0.11 μm during the coming decade.

The fabrication of the interconnect structure uses the ''damascene'' method. First a blanket layer of ILD is deposited and vias are anisotropically plasma etched. Titanium is deposited into the via. The titanium acts as an adhesion layer, but also improves the electrical contact resistance by consuming residual oxides from the surface of the underlying layer. It is important to deposit material all the way to the bottom of the structure during this step. The success of the deposition is measured by the bottom coverage which is defined as the ratio of Ti film thickness at the bottom of the via

*Paper pThpT-1 Bull. Am. Phys. Soc. **42**, 2026 (1997).
[†]Tutorial speaker.
[a)]Electronic mail: jhopwood@lynx.neu.edu

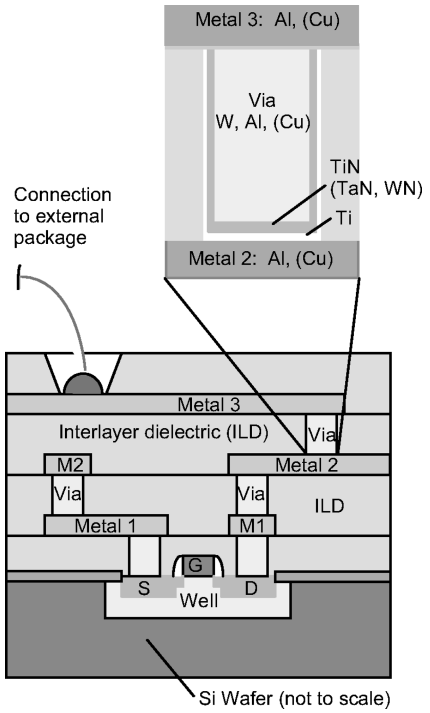

FIG. 1. A partial cross section of a simplified integrated circuit. The expanded view shows a via that is lined with Ti and TiN and subsequently filled with W or Al. Future materials are indicated in parentheses.

to the thickness deposited on the top surface of the ILD. Next the via receives a barrier layer of TiN that protects the ILD from corrosive effects of WF_6 during chemical vapor deposition of the tungsten via plug. Alternately, if aluminum is used as the plug material, the TiN acts as a wetting layer that allows the sputtered aluminum to be reflowed[3] into the via at elevated temperatures. In both cases, the TiN acts as a diffusion barrier between the plug and the ILD. The diffusion barrier must be conformal to the via and it should be as thin as possible so that very little cross sectional area is occupied by the somewhat resistive barrier material. Finally the low-resistivity via plug material is deposited. This material is progressing from W to Al, and eventually Cu. The overburden of metal present on the ILD after deposition of the plug is removed by chemical-mechanical polishing. In the single damascene process, these step are repeated for the deposition of the metal lines above the vias. A future alternative is the dual damascene process[4] in which the via and metal levels are etched simultaneously. Then both the via and the metal line are filled with conducting materials and planarized by CMP in the final step. The dual damascene process reduces the number of processing steps needed to fabricate a metal level, but the requirements on the deposition process are considerably more stringent.

Aluminum-0.5% Cu metallization is projected to be replaced by pure copper.[5] Copper has a lower bulk electrical resistivity than AlCu (1.7 vs 3.2 $\mu\Omega$-cm) so that the interconnect delay time (RC) may be decreased. Equally important is copper's ability to conduct higher current densities than AlCu without failure of the thin lines due to electromigration of the metal atoms. Since copper does not form a self-limiting oxide, copper interconnects will need to be completely enveloped in a passivating diffusion barrier, most likely consisting of Ta and TaN layers.

Although many technological challenges exist in the areas of lithography, low-permittivity dielectric materials and via etching, this paper will focus on the directional deposition of barrier and plug materials. There are three potential methods of interconnect deposition: Physical vapor deposition (PVD), chemical vapor deposition (CVD), and electroplating. The CVD methods use elevated temperatures or plasma[6] to dissociate precursor species. Filling or lining of high aspect ratio features is accomplished by fragmented precursor species with low sticking coefficients that are capable of reaching and depositing at the bottom of deep, narrow openings. While highly conformal films can be deposited using CVD, the cost and toxicity of the precursor materials remains an issue. Plating is also an effective way of filling high AR features. The plating baths, however, can be difficult to maintain, present a liquid waste hazard, and represent a departure from the semiconductor industry's preference for dry processing. PVD, and in particular sputtering, has long been the workhorse of the industry. The fundamental problem with sputtering, however, is the sputtered species are ejected from the solid target with a $\cos^n(\theta)$ angular distribution[7,8] which limits bottom coverage to approximately 0.2 in structures with 2:1 ARs. Physical collimation[9] of the sputtered flux by a honeycomb-shaped filter between the target and wafer improves film conformality by trapping sputtered species with large angle trajectories. Bottom coverage[10] of 2:1 features increases to 0.3–0.4, but the collimator significantly reduces the deposition rate and may create particles that reduce the yield of functional ICs.

II. IONIZED PHYSICAL VAPOR DEPOSITION (I-PVD)

I-PVD is a recent advance in PVD technology that achieves directional deposition of metals by ionizing the sputtered or evaporated metal atoms and collimating these ions with the plasma sheath adjacent to the wafer as shown in Fig. 2. A high electron density ($n_e \gg 10^{11}$ cm^{-3}), inert gas plasma between the target and the wafer is needed to ionize the metal vapor. Strong ionization of the metal occurs since the electron temperature depends primarily on the ionization potential of the inert gas (15.7 eV for argon) which is much greater than that of metals (6.0 and 7.7 eV for Al and Cu). The plasma source is commonly an electron cyclotron resonance plasma[11–13] or inductively coupled plasma.[14–17]

The average distance that a sputtered neutral will travel before being ionized dictates the design of an I-PVD system. Simple analysis of a sputtered neutral traversing a high density plasma gives the ionization mean free path[18,19] as $\lambda_{iz} = \nu_s / K_i n_e$ where ν_s is the velocity of the sputtered neutral and K_i is the ionization rate constant (see below). Atoms sputtered from the target exhibit a Thomson distribution[20] where the most probable energy is one half the surface binding energy ($\sim$1.5 eV for Al). Therefore, $\lambda_{iz} \sim 60$ cm in an Ar plasma where $T_e = 3$ eV and $n_e = 5 \times 10^{11}$ cm^{-3}. This analysis suggests two methods of generating a highly ionized, directional metal flux. First, if the inert gas pressure is quite low, the target-to-wafer distance must be quite long.

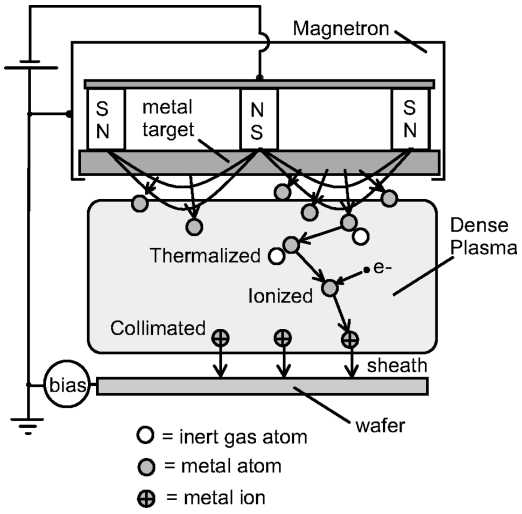

FIG. 2. A typical ionized PVD reactor sputters metal atoms into a high density plasma. Once thermalized, the atoms are ionized by electron impact. The ions diffuse to the wafer region where they are collimated by the plasma sheath and directionally deposited.

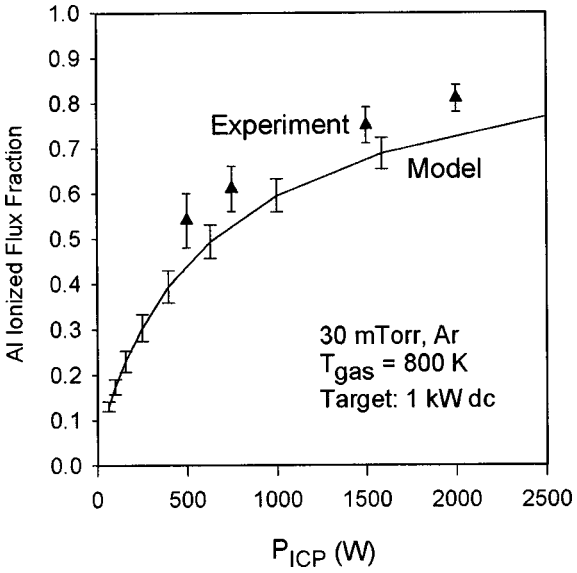

FIG. 3. Experimental ionization of a sputtered Al flux can exceed 80% in an argon inductively coupled plasma. The solid curve shows a global model for ionization of Al.

The second alternative is to increase the pressure such that the sputtered metal is collisionally thermalized by the inert background gas. If the metal is first thermalized ($\sim$0.05 eV), the ionization path length decreases to $\sim$10 cm and the target and substrate may be separated by as little as 10 cm.[16] I-PVD accomplished through thermalization, ionization and collimation (Fig. 2) will be the focus of the remainder of this paper.

The film coverage of trench and via structures[21] depends on many factors including resputtering of the surface by argon ions, redeposition of resputtered surface materials, ion enhanced mobility of surface atoms, and modified sticking coefficients due to oblique angles of incidence. The most obvious factor, however, is the fractional ionization of the metal flux incident on the wafer. Since metal ions are accelerated to the Bohm velocity by the plasma's presheath, the ion flux at the wafer is

$$\Gamma_i = 0.61[M^+]\cdot(k_B T_e/m_i)^{1/2}, \tag{1}$$

where $[M^+]$ is the metal ion density, m_i is the ion mass and T_e is the electron temperature. In contrast, the flux of thermalized neutral metal is

$$\Gamma_n = 1/4\nu_{\text{th}}[M] \tag{2}$$

where $\nu_{\text{th}}=(8k_B T_{\text{gas}}/\pi m)^{1/2}$ is the mean thermal velocity of the gas. Since $T_e \gg T_{\text{gas}}$, the fraction of ionized metal flux to a wafer is larger than the fraction of ionized metal in the plasma. For example, if $[M^+]/([M^+]+[M])$ is 0.3, the fraction of ionized metal flux is increased to $\Gamma_i/(\Gamma_i+\Gamma_n)$ $\sim$0.8. This means that it is not necessary to completely ionize the sputtered metal to create a highly ionized flux to the wafer.

To understand and optimize the I-PVD method, it is necessary to characterize the degree of metal ionization in the plasma. Several methods exist to determine the metal ionization including optical emission spectroscopy,[17,19] electrostatic separation of ion and neutral fluxes,[16,17] evaluation of the bottom fill in deep trench structures,[21,22] and the accumulating Langmuir probe.[19] The accumulating probe technique determines the metal ion density from the accumulated film thickness on a flat, floating probe using Eq. (1). Since the total film thickness is due to ions and neutrals, a second probe measurement is performed with no metal ionization (i.e., no high density plasma) to find the neutral metal flux [Eq. (2)] and the neutral density. This second experimental flux is subtracted from the total flux determined in the first experiment to yield the metal ion density.

Figure 3 shows the fraction of ionized metal flux to a 200 mm wafer positioned 15 cm from an AlCu target. The diameter of the inductively coupled plasma (ICP) for this IPVD reactor is 44 cm and the target diameter is 30 cm. The argon pressure was 30 mTorr such that thermalization of the aluminum flux occurred a few cm below the target. At the highest ICP power of 2 kW, the aluminum flux is composed of about 80% ions. A global model for the ionization process shown on the figure is described in the next section.

III. MODELING OF METAL IONIZATION

In this section a global (zero-dimensional, spatially averaged) model for metal-argon plasmas[23] is outlined. The strategy is to develop generation rates for argon excited states, argon ions, and metal ions, as well as radiative and diffusive loss rates. For a given gas pressure and electron density, the electron temperature and ion fraction are then self-consistently determined by balancing these generation and loss rates.

The model assumes that the sputtered metal is thermalized by collisions with the argon background gas. The three most important collisions responsible for the generation of metal ions in an inert gas plasma are electron impact ionization of the metal neutral, electron impact ionization of a

metal excited state, and Penning ionization by collision with an electronically excited argon atom. The specific collisions with the metal atom, M, are

$$M+e^- \xrightarrow{K_i} M^+ + 2e^-, \tag{3}$$

$$M^* + e^- \xrightarrow{K_i^*} M^+ + 2e^-, \tag{4}$$

$$\mathrm{Ar}^* + M \xrightarrow{K_p} M^+ + \mathrm{Ar} + e^-, \tag{5}$$

where K_i, K_i^*, and K_p are the rate constants for electron impact collisions and Penning ionization, respectively.

To determine the loss rate of M^+, it is observed that ionized PVD processes typically occur at gas pressures of 30 mTorr and the chamber radius is the order of $R \sim 20$ cm. The ratio of the ion density at the sheath edge to the central ion density is[24,25]

$$h_R = \frac{n_i(r=R)}{n_{io}} \approx \frac{0.8}{\sqrt{4+(R/\lambda_i)}} = 0.06, \tag{6}$$

where λ_i is the ion mean free path. Since the ion density near the wall of the chamber is negligible, we will use the solution to the ambipolar diffusion equation with the boundary condition that $n_i(\text{wall}) = 0$ to determine the ion lifetime[26] in the plasma to be

$$\frac{1}{\tau_i} = D_a \left[\left(\frac{\pi}{L} \right)^2 + \left(\frac{2.405}{R} \right)^2 \right], \tag{7}$$

where $D_a = k_B T_e \mu_+ / e$ is the ambipolar diffusion coefficient of M^+ in an inert gas and L is the distance between the wafer and the target. The mobility (μ_+) of various ions in Ar is calculated using the Langevin formula in the polarization limit.[27] Setting the generation rate of metal ions equal to the diffusive loss rate, one finds

$$K_p[\mathrm{Ar}^*][M] + K_i[e][M] + K_i^*[e][M^*] = \tau_i^{-1}[M^+]. \tag{8}$$

Since the rate constants for ionization of excited metal species (M^*) are generally not known, K_i^* will be set to zero such that two-step ionization is ignored. The ramifications of this approximation will be discussed later in this manuscript. The Penning ionization rate depends on the excited argon density [Ar*] which is produced by electron collisions

$$\mathrm{Ar} + e^- \xrightarrow{K_e} \mathrm{Ar}^* + e^-. \tag{9}$$

The loss rate of Ar* depends on the Penning ionization rate described by Eq. (5), diffusive losses characterized by the metastable diffusion lifetime

$$\frac{1}{\tau_M} = D_M \left[\left(\frac{\pi}{L} \right)^2 + \left(\frac{2.405}{R} \right)^2 \right], \tag{10}$$

where D_M is the metastable diffusion coefficient.[28] Other loss mechanisms for Ar* are imprisoned resonant radiative decay,[29] which will be denoted by the lifetime τ_r, and collisional ionization of the excited states

$$\mathrm{Ar}^* + e^- \xrightarrow{K_c} \mathrm{Ar}^+ + 2e^-. \tag{11}$$

The particle balance equation for the generation and loss of excited argon is

$$K_e[e][\mathrm{Ar}] = [\mathrm{Ar}^*]\left\{ K_c[e] + K_p[M] + \tau_m^{-1} + \tau_r^{-1} \right\} \equiv \tau^{-1}[\mathrm{Ar}^*]. \tag{12}$$

Noting that the total metal density is $[M]_0 = [M] + [M^+]$, the metal ion fraction in a plasma with electron density $[e]$ is

$$\frac{[M^+]}{[M]_0} = \frac{(K_i + K_p K_e \tau[\mathrm{Ar}])\tau_i[e]}{1 + (K_i + K_p K_e \tau[\mathrm{Ar}])\tau_i[e]}. \tag{13}$$

Equation (13) is an implicit expression for the ion fraction since the neutral metal density $[M]$ appears in the factor τ. A meaningful solution to Eq. (13) requires a knowledge of the electron temperature since the electron-impact rate constants are determined from

$$K_j(T_e) = \langle \sigma_j v \rangle = \int_{E_t}^{\infty} v \sigma_j(E) f(T_e, E) dE, \tag{14}$$

where σ_j are the collision cross sections for the various reactions discussed above, v is the electron velocity, and $f(T_e, E)$ is the electron energy distribution function. The electron temperature can be self-consistently determined by imposing quasi-neutrality $[e] = [\mathrm{Ar}^+] + [M^+]$. This requires a calculation of the argon ion density from

$$K_a[\mathrm{Ar}][e] + K_c[\mathrm{Ar}^*][e] = \tau_{i(\mathrm{Ar}^+)}^{-1}[\mathrm{Ar}^+], \tag{15}$$

where the rate constant K_a represents the single-step ionization process

$$\mathrm{Ar} + e^- \xrightarrow{K_a} \mathrm{Ar}^+ + 2e^-. \tag{16}$$

Metals of interest for interconnect technology include Al, Cu, Ta, and Ti. The Penning ionization rate constant for these metals is $K_p = \sigma_p \nu_{\mathrm{th}}$, where σ_p is the Penning cross section. In the absence of experimentally measured Penning cross sections for metals of interest, published data[30] for Zn and Cd will be scaled by the square of the atomic radii. This is a crude approximation to the actual cross sections, but the ionization of metal in a high density argon discharge is primarily due to electron impact ionization. Relatively large errors in the Penning cross section, therefore, have little effect on the calculated ionization of metals in I-PVD.[2]

The fraction of ionized metal may be determined from the expressions outlined above for a given argon gas density and temperature, total metal density, electron density and chamber size (R,L). The rate constants are calculated using an initial guess for the electron temperature. Then Eqs. (13) and (15) are used to find the argon ion and metal ion densities. The sum of these two ion densities is compared with the chosen electron density, and the electron temperature is iteratively adjusted until charge neutrality is achieved. To hasten convergence to the solution, the rate constants are expressed in an Arrhenius form by numerically integrating cross sections from the literature using Eq. (14) and fitting the results to

$$K(T_e) = K_0 \exp(-E_0/T_e). \tag{17}$$

TABLE I. Rate constants and mobilities for species in ionized PVD plasmas.

	$K_0\times10^{-8}$ (cm^3/s)	E_0 (eV)	Reference	μ_0 at STP ($cm^2\ v^{-1}\ s^{-1}$)
K_e: Ar → Ar*	2.2	12.4	de Heer *et al.* (Ref. 33)	2.7(Ref. 28)
K_c: Ar* → Ar^+	21	5.3	Vriens (Ref. 34)	1.6 (Refs. 31 and 32)
K_a: Ar → Ar^+	12.3	18.68	Rapp *et al.* (Ref. 35)	1.6
K_i: Al → Al^+	12.3	7.23	Shimon *et al.* (Ref. 36)	2.7 (Ref. 27)
K_i: Ti → Ti^+	23.4	7.25	Lennon *et al.* (Ref. 37)	2.3 (Ref. 27)
K_i: Cu → Cu^+	5.62	8.77	Lotz (Ref. 38)	2.2 (Ref. 27)
K_i: C → C^+	4.0	12.6	Lotz (Ref. 38)	3.6 (Ref. 27)

Table I lists the constants K_0 and E_0 used in this model and references to the original cross section data. Also included is the mobility of the product species for each collision.[27,28,31–38]

The results from this model are compared with experimental measurements in Fig. 3. The elevated gas temperature used in the model (800 K) is due to energy transferred from the energetic sputtered aluminum atoms to the argon gas during thermalization.[39,40] The error bars for the model show the sensitivity of the calculation to a 20% uncertainty in the measured ionization cross section for aluminum. This comparison shows that the global model reasonably predicts the ion flux fraction within the inherent inaccuracies of the model and the experiment. One possible reason for the model's consistently under-predicted ionization is the omission of two-step metal ionization ($M+e\rightarrow M^*+e$; $M^*+e\rightarrow M^++2e$) which may be a significant additional source of M^+.

Figure 4 shows the modeled ionization of various metals that are either currently used or projected for use in IC interconnects. The error bars on the Cu data indicate the 30% uncertainty in the ionization cross section. Notice that the ion fraction is a few percent when the electron density is the order of 10^{10} cm^{-3}. This is a typical ionization level for conventional sputtering and is primarily due to Penning ionization.[41] At higher electron density, however, the excited-state argon density is inhibited by electron collisions[42] [Eq. (11)] such that electron impact ionization dominates the Penning ionization of M.[23] At electron densities greater than $\sim10^{11}$ cm^{-3}, the important parameters that determine how completely a metal flux will be ionized in I-PVD are the electron impact ionization cross section, ionization potential, and the mobility of M^+ in argon. The first two factors relate to the generation of metal ions and the mobility sets the loss rate. For example, although Ti has a higher ionization threshold than Al, the relative ionization of Ti atoms is higher since the cross section is twice that of Al while the mobility of Ti^+ is somewhat lower. Copper, on the other hand, has a much lower cross section and a higher ionization potential than Ti or Al. These factors make Cu more difficult to ionize. Finally, although not related to interconnects, carbon ionization is included in the figure to demonstrate that atoms with high ionization potential (11.26 eV for C) and high ion mobilities are not significantly ionized in an argon plasma even at densities approaching 10^{13} cm^{-3}.

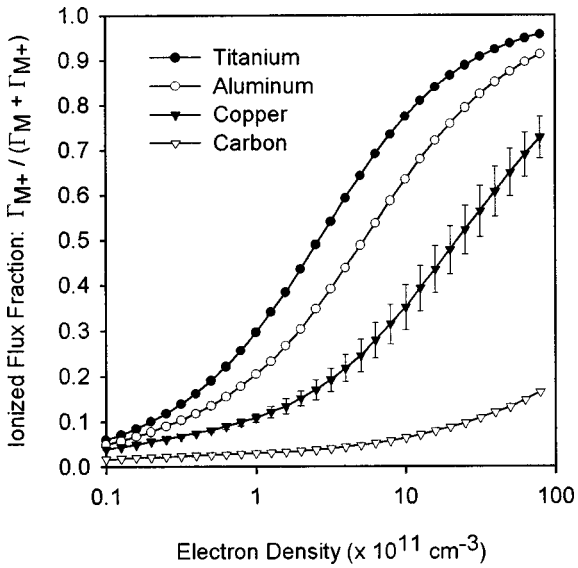

FIG. 4. Comparison of the modeled ionized flux fraction for several metals used for IC interconnects. Metals with a large ionization cross section, low ionization potential, and low ion mobility are the most highly ionized.

IV. SPATIAL VARIATION OF METAL IONS AND NEUTRALS

Although the global model presented in the previous section is useful for developing a basic understanding of I-PVD, the model assumes a spatially homogeneous discharge. Experimental measurements of the radial and axial variation[19] of [Al] and [Al^+] are presented in this section to improve on this simple picture. To determine the axial variation of metal species, the accumulating Langmuir probe technique was used to measure the density of aluminum atoms and ions between the sputter target at $z=0$ and the plane of the wafer at $z=14$ cm. The measurement method is not valid in the region close to the target since the sputtered metal atoms are not thermalized and Eq. (2) does not apply. For z greater than ~2 to 3 cm, however, the metal is mostly thermalized in a 30 mTorr argon plasma[43,44] and the gas phase metal density can be determined as shown in Fig. 5.

The neutral Al density in Fig. 5 is greatest near the target and decreases nearly exponentially towards the wafer. The Al^+ density, however, is sustained by electron impact throughout the plasma volume and remains relatively constant along the axis of the chamber. These data show that high fractions of metal ionization are attained at the wafer by the combined effects of (1) neutral density decay due to dif-

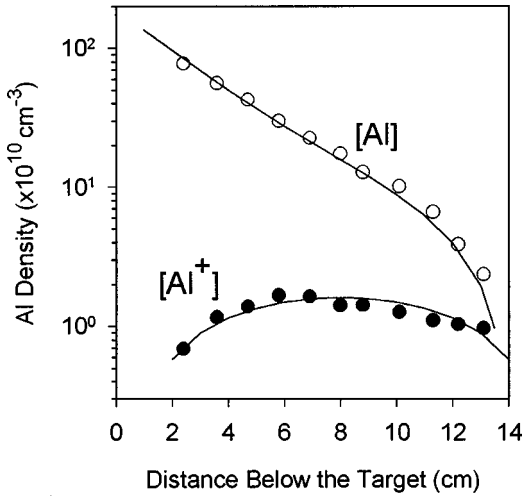

FIG. 5. Measurement of the aluminum ion and neutral density along the axis of an I-PVD reactor demonstrates that high ion fractions are achieved through he decay of the neutral metal density and sustained volume generation of metal ions. Solid curves are diffusion models described in the text. The target diameter for this experiment was 75 mm.

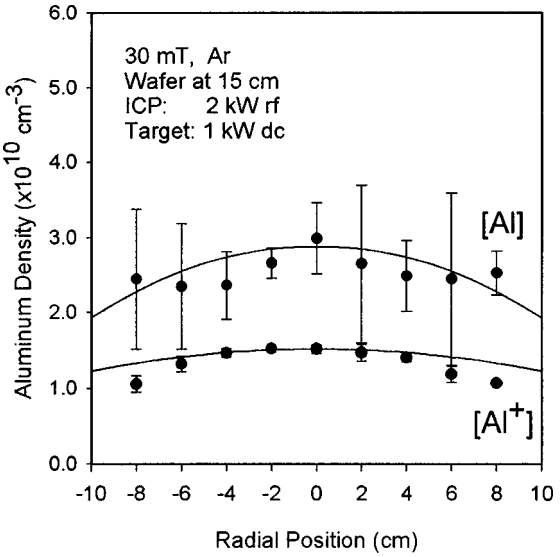

FIG. 6. The radial variation of Al and Al^+ suggests diffusive transport of both species. Solid curves are diffusion models described in the text.

fusive losses of metal to the chamber walls, and (2) approximately uniform volume generation of metal ions extending down to the region near the wafer.

Using the same measurement technique, the radial distributions of Al and Al^+ adjacent to the surface of a 200 mm wafer were determined and are plotted in Fig. 6. Notice that although the bulk ionization fraction ($[Al^+]/[Al]+[Al^+]$) is only 0.3, the ionized flux fraction is about 0.8 as shown in Fig. 3. The aluminum ion density is peaked at the center of the wafer and decreases at larger radii. This is a typical diffusion-dominated distribution of ions as discussed below.

To aid in the understanding of ionization in an I-PVD reactor, a simple model is proposed. Since the sputtered metal atoms are thermalized in the first few centimeters near the target, transport of metal atoms to the wafer is diffusive rather than ballistic. From this observation it is reasonable to attempt a solution to the diffusion equation for metal atoms $[\nabla^2 n_M(r,z)=0]$ in a cylinder (R, L) with the boundary condition that $[M] = 0$ at the chamber walls. The sputtering source of M is modeled with a boundary adjacent to the target that is the sum of k disks, each of constant Al density and concentric about the central axis at $z\sim 0$,

$$n_M(r,z\sim 0)=N_0\sum_{i=1}^{k} A_i[1-u(r-b_i)], \tag{18}$$

where u is the unit step function and the constants b_i and A_i are chosen to match the erosion profile of the target. The diffusion solution is

$$n_M(r,z)=2N_0\sum_{i=1}^{k} A_i \frac{b_i}{R}\sum_{j=0}^{\infty}\frac{J_1(x_{0j}b_i/R)}{x_{0j}J_1^2(x_{0j})}J_0\left(\frac{x_{0j}r}{R}\right) \times\left(\frac{\exp(-k_z z)-\exp(k_z(z-2L))}{1-\exp(-2k_z L)}\right), \tag{19}$$

where J_n is the n^{th}-order Bessel function of the first kind, $k_z=x_{0j}/R$, and $J_0(x_{0j})=0$. The modeled aluminum neutral density [Eq. (19)] is plotted along with the experimental measurements in Figs. 5 and 6. Only the magnitude of the density (N_0) was scaled to fit the data. The agreement of the diffusion model for the Al distribution is within the accuracy of the experiment. The right hand side of Fig. 7 shows a contour plot of the neutral density [Al] superimposed on a sketch of an I-PVD reactor with $R=22$ cm and $L=15$ cm.

It has previously been shown that sputtered atoms must be thermalized if ionization is to occur within the confines of the I-PVD reactor. Since the metal ions are thermalized, it is reasonable to assume that the ion density distribution will be diffusive as well. The Klyarfeld parabolic approximation[25] has been shown to predict the distribution of ions in inductively coupled plasmas.[45] By combining the Klyarfeld solution for a long tube $n_T(r)$ with the solution for an infinite slab geometry $n_S(z)$, an estimate of the ion density within a cylinder is $n_{M^+}(r,z)=n_T(r)n_S(z)$ where

$$n_T(r)\approx n_{io}\left(1-(1-h_R)\left(\frac{r}{R}\right)^2\right), \tag{20}$$

$$n_S(z)\approx n_{io}\left(1-(1-h_l)\left(\frac{z-L/2}{L/2}\right)^2\right), \tag{21}$$

$$h_l\approx\frac{0.86}{\sqrt{3+L/2\lambda_i}}, \tag{22}$$

and h_R is given in Eq. (6). Figures 5 and 6 show that this approximate solution for aluminum ion density agrees well with respect to z but predicts a metal ion density that is more uniform along the radial direction than experimentally observed. The left hand side of Fig. 7 shows a contour plot of the Klyarfeld parabolic approximation within a typical Al^+ I-PVD reactor at 10 mTorr. Finally, although the uniformity of the deposition rate over 200 mm wafers was typically 7%–13%, the fraction of ionized flux is much more uniform since the diffusion dominated metal and metal ion densities decrease radially at similar rates. There are several unifor-

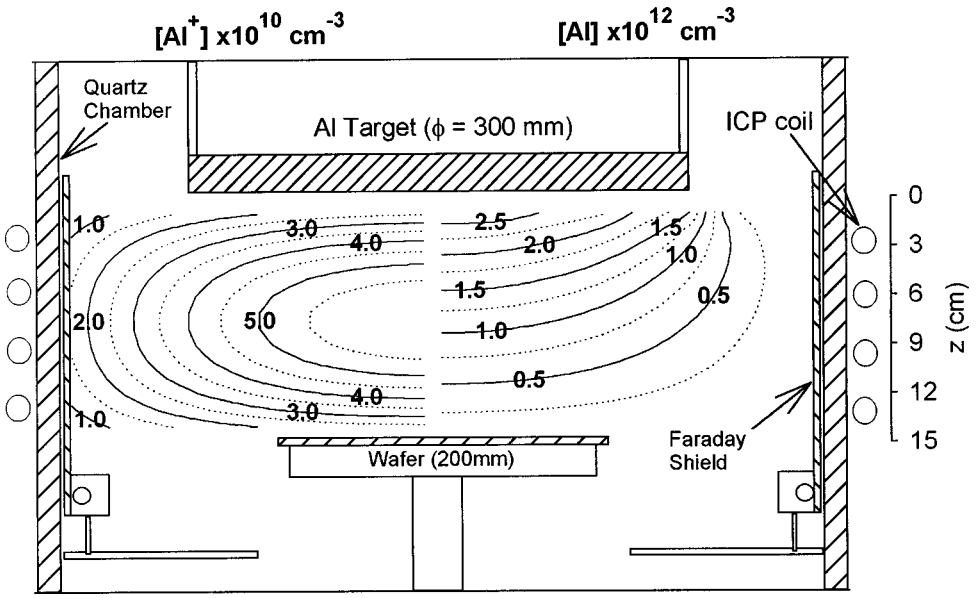

FIG. 7. Contour plots of aluminum neutral and ion density in a 44 cm diameter I-PVD reactor.

mity issues yet to be resolved, but bottom coverage (which is proportional to ionization fraction) should be quite consistent across large wafers.

V. CONCLUSION

Ionized physical vapor deposition is a viable technique for the fabrication of high aspect ratio interconnects for future generations of integrated circuits. The advantages of I-PVD over the alternative methods are numerous: The metal source is a nontoxic low-cost solid, the process does not produce chemical wastes, sputtering is a very clean process, and sputtering has a well-established technology base in the IC fabrication industry. The most promising applications for I-PVD are for the deposition of liners and barriers—the refilling of high aspect ratio vias with metal is an area where additional research is required.

Ionization of sputtered species is most effective when the ionization potential of the inert gas is much greater than the metal. Metals with low ion mobility will also exhibit higher fractional ionization. Reactor geometry is shown to influence ionization. These factors include designing the reactor with sufficient target-to-wafer spacing so that thermalization of sputtered atoms occurs within the high density plasma. Uniformity of the deposition rate and bottom coverage depend on the distribution of ions and the fraction of ionized flux. The ion flux fraction is inherently uniform since diffusive transport applies to both metal neutrals and ions. Further research and development are needed to control the uniformity of ions at the wafer. Finally, while the body of knowledge for directional metal deposition using inert gas I-PVD is maturing, the physics, gas-phase chemistry, and process technology of nitride deposition (TiN, TaN, and WN) is not yet well-understood for I-PVD processes.

ACKNOWLEDGMENTS

The author wishes to acknowledge the assistance of M. Dickson and G. Zhong.

This work is currently supported by the National Science Foundation and U.S. Department of Energy under Grant No. DMR-9712988.

[1] *National Technology Roadmap for Semiconductors* (Semiconductor Industry Association, San Jose, CA, 1994).
[2] S. P. Murarka, *Metallization: Theory and Practice for VLSI and ULSI* (Butterworth-Heinemann, Boston, 1993).
[3] H. Liao and T. S. Cale, J. Vac. Sci. Technol. B **14**, 2615 (1996), and references therein.
[4] S. M. Rossnagel, J. Vac. Sci. Technol. B **13**, 125 (1995).
[5] P. F. Cheung, S. M. Rossnagel, and D. N. Ruzic, J. Vac. Sci. Technol. B **13**, 203 (1995).
[6] J. Faltermeier, A. Knorr, R. Talevi, H. Gundlach, K. A. Kumar, G. G. Peterson, A. E. Kaloyeros, J. J. Sullivan, and J. Loan, J. Vac. Sci. Technol. B **15**, 1758 (1997).
[7] H. H. Andersen, B. Stenum, T. Sorensen, and H. Whitlow, Nucl. Instrum. Methods Phys. Res. B **6**, 459 (1985).
[8] Y. Yamamura and M. Ishida, J. Vac. Sci. Technol. A **13**, 101 (1995).
[9] S. M. Rossnagel, D. Mikalsen, H. Kinsohita, and J. J. Cuomo, J. Vac. Sci. Technol. A **9**, 261 (1991).
[10] R. Powell (private communication, 1996).
[11] T. Ono, C. Takahashi, and S. Matsuo, Jpn. J. Appl. Phys. **23**, L534 (1984).
[12] W. M. Holber, J. S. Logan, J. J. Grabarz, J. T. C. Yeh, J. B. O. Caughman, A. Sugerman, and F. E. Turene, J. Vac. Sci. Technol. A **11**, 2903 (1993).
[13] C. Doughty, S. M. Gorbatkin, T. Y. Tsui, G. M. Pharr, and D. L. Medlin, J. Vac. Sci. Technol. A **15**, 2623 (1997).
[14] M. Yamashita, J. Vac. Sci. Technol. A **7**, 151 (1989).
[15] M. Yamashita, J. Vac. Sci. Technol. A **7**, 2752 (1989).
[16] S. M. Rossnagel and J. Hopwood, Appl. Phys. Lett. **63**, 3285 (1993).
[17] S. M. Rossnagel and J. Hopwood, J. Vac. Sci. Technol. B **12**, 449 (1994).
[18] S. M. Rossnagel, Thin Solid Films **263**, 1 (1995).
[19] M. Dickson and J. Hopwood, J. Vac. Sci. Technol. A **15**, 2307 (1997).
[20] M. W. Thompson, Philos. Mag. **18**, 377 (1968).
[21] S. Hamaguchi and S. M. Rossnagel, J. Vac. Sci. Technol. B **14**, 2603 (1996).
[22] C. A. Nichols, S. M. Rossnagel, J. Vac. Sci. Technol. B **14**, 3270 (1996).
[23] J. Hopwood and F. Qian, J. Appl. Phys. **78**, 758 (1995).
[24] M. A. Lieberman and A. J. Lichtenberg, *Principles of Plasma Discharges*

and Materials Processing (Wiley, New York, 1994), p. 140.
[25]V. A. Godyak, *Soviet Radio Frequency Discharge Research* (Delphic, Falls Church, VA, 1986), p. 79ff.
[26]B. E. Cherrington, *Gaseous Electronics and Gas Lasers* (Pergamon Press, Oxford, 1979), p. 119.
[27]L. M. Chanin and M. A. Biondi, Phys. Rev. **107**, 1219 (1957).
[28]A. H. Futch and F. A. Grant, Phys. Rev. **104**, 356 (1956).
[29]T. Holstein, Phys. Rev. **83**, 1159 (1951).
[30]L. A. Riseberg, W. F. Parks, and L. D. Schearer, Phys. Rev. A **8**, 1962 (1973).
[31]M. A. Biondi and L. M. Chanin, Phys. Rev. **94**, 910 (1954).
[32]K. B. McAfee, D. Siple, and D. Edelson, Phys. Rev. **160**, 130 (1967).
[33]F. J. de Heer, R. H. Jansen, and W. van der Kaay, J. Phys. B: Atom. Molec. Phys. **12**, 979 (1979).
[34]L. Vriens, Phys. Lett. **8**, 260 (1964).
[35]D. Rapp and P. Englander-Golden, J. Chem. Phys. **43**, 1464 (1965).
[36]L. L. Shimon, E. I. Nepiipov, and I. P. Zapesochnyi, Sov. Phys. Tech. Phys. **20**, 434 (1975).
[37]M. A. Lennon, K. L. Bell, H. B. Gilbody, J. G. Hughes, A. E. Kingston, M. J. Murray, and F. J. Smith, J. Phys. Chem. Ref. Data **17**, 1285 (1988).
[38]W. Lotz, Z. Phys. **232**, 101 (1970), and references therein.
[39]M. Dickson, F. Qian, and J. Hopwood, J. Vac. Sci. Technol. A **15**, 340 (1997).
[40]S. M. Rossnagel, J. Vac. Sci. Technol. A **6**, 19 (1988).
[41]J. W. Coburn and E. Kay, Appl. Phys. Lett. **18**, 435 (1971).
[42]B. E. Cherrington, *Gaseous Electronic and Gas Lasers* (Pergamon Press, Oxford, 1979), p. 169.
[43]A. Gras-Marti and J. A. Valles-Abarca, J. Appl. Phys. **54**, 1071 (1983).
[44]L. T. Ball, I. S. Falconer, D. R. McKenzie, and J. M. Smelt, J. Appl. Phys. **59**, 720 (1986).
[45]N. Forgotson, V. Khemka, and J. Hopwood, J. Vac. Sci. Technol. B **14**, 732 (1996).